Aβ40-Lactam(D23/K28) Models a Conformation Highly Favorable for Nucleation of Amyloid†

Kimberly L. Sciarretta,‡ David J. Gordon,§ Aneta T. Petkova,|| Robert Tycko,|| and Stephen C. Meredith*,§,⊥

Departments of Molecular Genetics and Cell Biology, Biochemistry and Molecular Biology, and Pathology, The University of Chicago, Chicago, Illinois 60637, and Laboratory of Chemical Physics, National Institute of Diabetes and Digestive and Kidney Diseases, National Institutes of Health, Bethesda, Maryland 20892-0520

Received November 30, 2004; Revised Manuscript Received February 10, 2005

ABSTRACT: Recent solid-state NMR data (*1*) demonstrate that Aβ_{1-40} adopts a conformation in amyloid fibrils with two in-register, parallel β-sheets, connected by a bend structure encompassing residues D^{23}VGSNKG^{29}, with a close contact between the side chains of Asp23 and Lys28. We hypothesized that forming this bend structure might be rate-limiting in fibril formation, as indicated by the lag period typically observed in the kinetics of Aβ_{1-40} fibrillogenesis. We synthesized Aβ_{1-40}-Lactam(D23/K28), a congener Aβ_{1-40} peptide that contains a lactam bridge between the side chains of Asp23 and Lys28. Aβ_{1-40}-Lactam-(D23/K28) forms fibrils similar to those formed by Aβ_{1-40}. The kinetics of fibrillogenesis, however, occur without the typical lag period, and at a rate ≈1000-fold greater than is seen with Aβ_{1-40} fibrillogenesis. The strong tendency toward self-association is also shown by size exclusion chromatography in which Aβ_{1-40}-Lactam(D23/K28) forms oligomers even at concentrations of ≈1−5 μM. Under the same conditions, Aβ_{1-40} shows no detectable oligomers by size exclusion chromatography. Our data suggest that Aβ_{1-40}-Lactam(D23/K28) could bypass an unfavorable folding step in fibrillogenesis, because the lactam linkage "preforms" a bendlike structure in the peptide. Consistent with this view Aβ_{1-40} growth is efficiently nucleated by Aβ_{1-40}-Lactam(D23/K28) fibril seeds.

β-Amyloid (Aβ)[1] peptides are derived from the proteolytic cleavage of the β-amyloid precursor protein, forming Aβ_{1-40}, Aβ_{1-42}, and other less abundant products (*2*, *3*). Aβ peptides, which constitute the most abundant protein component of neuritic plaques in Alzheimer's disease, assemble into fibrils with high β-sheet content. In this respect, Aβ fibrils resemble those formed by other proteins involved in other neurodegenerative diseases, including Huntington, Parkinson, and prion diseases. Fibril-forming proteins lack sequence similarity, but the fibrils are believed to share some structural characteristics derived from their β-sheet content (*4*), such as protease resistance and the ability to bind thioflavin (*5*, *6*) and Congo Red dyes (*7*−*9*).

The kinetics of Aβ_{1-40} fibrillogenesis show a long lag phase, in which no fibrils are formed, followed by rapid polymerization of the peptide into fibrils. The lag phase has been attributed to a rate-limiting step that consists of high-order oligomerization and/or conformational changes (*10*, *11*). Because of the high propensity of Aβ peptides to aggregate into insoluble fibrils and the temporal instability of intermediates in the pathway to fibril formation, traditional biophysical techniques are difficult to apply, and consequently little is know of the structure of these intermediates. A micelle-like oligomer has been proposed as an intermediate in Aβ fibrillogenesis (*12*, *13*). Small oligomers have been studied in permeabilization of lipid bilayers suggesting a mechanism of pathogenesis (*14*). Small angle neutron scattering has demonstrated micelle-like intermediates in β-amyloid protein fibril assemblies; these have been shown to contain 30−50 Å monomers and have elongated geometries (*15*). In other studies, Aβ fibrillogenesis was shown to involve conformational changes leading to the formation of extended β-sheets and proceeding through an oligomeric α-helix-containing intermediate (*16*).

† We thank the NIH Molecular Cell Biology Training Grant (NIH/NIGMS T32 GM07183, KLS), American Federation of Aging Research (Glenn/AFAR 2004, KLS) and the NIH Medical Scientist Training Grant (5 T32 GM07281, DJG) and the Alzheimer's Association (IIRG 98-1344, SCM) and NIH (RO1 NS042852, SCM) for support of this work.

* Corresponding author. Mailing address: Department of Pathology, The University of Chicago, 5841 S. Maryland Ave., Chicago, IL 60637. Tel: 773-702-1267. Fax: 773-834-5251. E-mail: scmeredi@uchicago.edu.

‡ Department of Molecular Genetics and Cell Biology, The University of Chicago.

§ Department of Biochemistry and Molecular Biology, The University of Chicago.

|| National Institutes of Health.

⊥ Department of Pathology, The University of Chicago.

[1] Abbreviations: 1D, one-dimensional; Aβ, β-amyloid peptide; BOP, benzotriazolyl-*N*-oxytris-(dimethyl-amino)phosphonium hexafluorophosphate; DIEA, diisopropylethylamine; DMS, dimethyl sulfide; DMSO, dimethyl sulfoxide; EDT, ethanedithiol; ESI, electrospray ionization; FMOC, 9-fluorenylmethoxycarbonyl; fpRFDR-CT, finite-pulse radio frequency driven recoupling; HBTU, 2-(1*H*-benzotriazol-1-yl)-1,1,3,3-tetramethyluronium hexafluorophosphate; HFIP, hexafluoroisopropanol; HOBT, *N*-hydroxybenzotriazole; HPLC, high performance liquid chromatography; MAS, magic-angle spinning; MALDI-TOF, matrix-assisted laser desorption ionization time of flight; NHS-oFMOC, 9-fluorenylmethyl succinimidyl carbonate; NMP, *N*-methylpyrrolidinone; PBS, phosphate buffered saline; REDOR, rotational echo double resonance; RP-HPLC, reverse-phase high performance liquid chromatography; tBOC, *tert*-butoxycarbonyl; TFA, trifluoroacetic acid.

10.1021/bi0474867 CCC: $30.25
Published on Web 03/30/2005

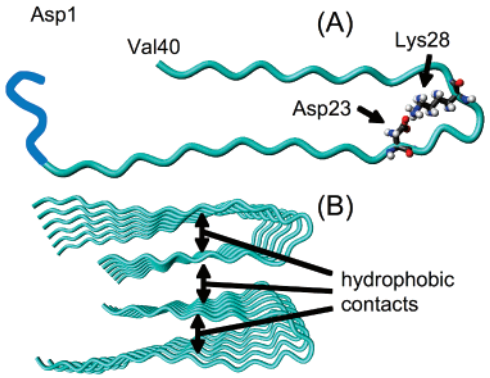

FIGURE 1: (Modified from Petkova et al. (*1*).) Structural model for Aβ_{1-40} fibril derived from energy minimization using constraints based on solid-state NMR data (*1*). (A) Peptide backbone conformation in the fibrils, showing a disordered N-terminal segment (blue), two β-strand segments (residues 10−22 and 30−40), and the bend segment (residues 23−29) containing oppositely charged Asp23 and Lys28. (B) Cross-sectional view of a piece of the Aβ_{1-40} protofilament, in which peptide molecules assemble into a four-layered parallel β-sheet structure, stabilized by hydrophobic contacts within and between the two molecular layers.

We have taken a model peptide approach to study critical conformational changes in the fibrillogenesis pathway. Solid-state NMR data (*17*−*20*) have demonstrated that the peptides in fibrils formed by Aβ_{10-35} and Aβ_{1-40} are aligned in parallel, in-register, β-sheets. Earlier studies used dipolar recoupling NMR methods to measure distances in these peptides between labels (peptides singly or doubly labeled with ^{13}C or ^{15}N), mainly in the backbone. Peptides containing single ^{13}C-carbonyl labels had intermolecular ^{13}C−^{13}C distances of approximately 5 Å at many positions in the peptide from Tyr10 to Val40. Results such as these were most consistent with parallel alignment of β-sheets. Chemical shift data also supported the conclusion of β-sheet structure for most residues in this region.

More recently, a detailed structural model for fibrillar Aβ_{1-40} was proposed from continued data accumulation and constrained energy minimization (*1*). This model is consistent with data from NMR studies including measurements of intermolecular distances using fpRFDR-CT (*19*), DRAWS (*17*), MQ ^{13}C NMR spectra (*20*), torsion angle constraints (*21*), and ^{13}C and ^{15}N chemical shift and line width measurements from 2D spectroscopy (*1*), as well as fibril mass per length from electron microscopy (*22*) and X-ray diffraction data (*23*). According to this model (shown in Figure 1), residues 10−22 and 30−40 form two β-strands in Aβ_{1-40} fibrils, which are connected by a bend structure encompassing residues D^{23}VGSNKG^{29}. This bend differs from a β-turn. Whereas a β-turn, defined by a set of backbone torsional angles, contains a hydrogen bond between backbone atoms, the bend structure in Aβ fibrils occurs in the "side-chain dimension" because it is defined and stabilized by side-chain interactions, both hydrophobic interactions and a salt bridge (between Asp23 and Lys28 in Figure 1), between the two separate, parallel β-sheets. Hence, a single molecular layer in this model is a double β-sheet. The first 10 residues of Aβ_{1-40} are structurally disordered in the fibril. According to this model, the protofilament could be constructed from two molecular layers, in which residues 30−40 create a hydrophobic surface for intermolecular interactions. Other investigators have also presented data in support of a non-β-sheet structure in the central portion of Aβ peptides. Solution-state NMR suggested a turn at positions 21−24 (*24*) or between 22−25, 24−27, 27−30, and 30−33 (*25*) of Aβ_{10-35}, or 20−26 of Aβ_{1-40} (*26*) in soluble, monomeric form, while molecular modeling and molecular dynamic simulations also suggest a bend or turn in this region of Aβ_{10-35} (*27*). In addition, proteolysis experiments and hydrogen/deuterium exchange of Aβ_{1-40} fibrils support the model of an unstructured, solvent-exposed N-terminus, and a structured core in the remainder of the peptide in fibrils (*28*, *29*). Proline mutagenesis (*30*) supported a model in which residues 22, 23, 29, and 30 appear to be involved in turn region. More recently, Török et al. (*31*) used electron paramagnetic resonance spectroscopy to confirm an in-register Aβ-sheet structure for Aβ_{1-40} fibrils, and demonstrated that the region around residues 23−26 of Aβ_{1-40} were more dynamic than surrounding β-sheet regions, which was compatible with a bend or turn in this region.

In this paper, we first report solid-state NMR data for salt bridge formation from the side-chain interactions of residues Asp23 and Lys28. Thereafter, we test the hypothesis that a rate-limiting step in fibrillogenesis is the conformational change similar to the "bend" seen in the fibril. To test this hypothesis, we have designed a congener Aβ_{1-40} peptide that contains a lactam bridge between the side chains of Asp23 and Lys28, and thus is intended to model the structure proposed by Petkova et al. (*1*). If the congener peptide models a structure similar to that in the Aβ fibrils, we would predict that it would form fibrils resembling the un-cross-linked Aβ_{1-40} peptide, but at much greater rates. We show that this congener does indeed form fibrils similar to that of Aβ_{1-40} but at ≈1000-fold greater rate. We also demonstrate that fibril formation by this lactam-containing peptide occurs without a lag period, suggesting that fibrillogenesis by the lactam-containing congener of Aβ_{1-40} bypasses the rate-limiting step in fibrillogenesis of un-cross-linked Aβ_{1-40}.

EXPERIMENTAL PROCEDURES

Peptide Synthesis and Purification. Aβ_{1-40} (NH_2-DAEFRHDSGY^{10}EVHHQKLVFF^{20}AEDVGSNKGA^{30}IIGLMVGGVV^{40}-COOH) was synthesized using modified 9-fluorenylmethoxycarbonyl (FMOC) and HBTU/HOBT (Fastmoc) chemistry on an Applied Biosystems (Foster City, CA) model 433A instrument. Peptides were cleaved from the resin using 9 mL of TFA plus 0.5 mL of thioanisole, 0.3 mL of EDT, and 0.2 mL of anisole for 1.5 h at 22 °C. Peptides were purified by RP-HPLC on a preparative C18 (Zorbax) column at 60 °C. Peptide purity was greater than 98% by analytical HPLC. The molecular mass of the peptide was verified by ESI and MALDI-TOF mass spectrometry.

A congener of Aβ_{1-40} was synthesized with an amide cross-link between the side chains of Asp23 and Lys28 (Aβ_{1-40}-Lactam(D23/K28)) using standard tBOC chemistry. The procedure for forming the lactam cross-link is based on the methods described in detail elsewhere (*32*). Briefly, the peptide chain was elongated using tBoc chemistry; α-Boc-Asp(β-OFm)-OH (Bachem) and α-Boc-Lys(ϵ-Fmoc) (Bachem) were used for residues to be cross-linked.

After Asp23 had been incorporated into the chain (α-BOC group remaining on Asp23), the Asp23 and Lys28 side chains were deprotected with piperidine (20%, v/v in NMP, 23 min,

22 °C) and coupled using benzotriazolyl-*N*-oxytris-(dimethylamino)phosphonium hexafluorophosphate (BOP) reagent (*33*), with the addition of DIEA and NMP for 4 h to form an amide bond between the β-carbon of Asp23 and the ε-nitrogen of Lys28. Coupling continued for 2 h, after which the reaction vessel was drained, additional BOP, NMP, and DIEA were added, and the reaction was allowed to proceed for another 2 h. Formation of the cross-link was later confirmed by ESI and MALDI-TOF mass spectrometry. After formation of the lactam cross-link, the peptide-resin was replaced in the synthesizer, and the remainder of the peptide chain was elongated using standard tBOC chemistry. For solid-state NMR experiments, 1-^{13}C-valine was incorporated as Val18 of this peptide. 1-^{13}C-Val (≥97% isotopic purity) was purchased from Cambridge Isotopes (Andover, MA) and was protected with the FMOC group by Midwest Biotech. Peptides made by tBOC chemistry were cleaved from the resin using anhydrous HF in an Immuno-Dynamics (La Jolla, CA) HF apparatus, using 10 mL of HF also containing 1 mL of *p*-cresol and 1 mL of DMS per 1 g of resin for 1 h at −3 to −5 °C. A 0.5 mmol scale reaction gave approximately ≈200 mg of crude peptide, of which only ≈5−8 mg of purified product could be obtained. The low yield was attributable to the high propensity of the peptide to aggregate, which made it difficult to separate the peptide from impurities. Nevertheless, a procedure was found to isolate pure peptide, as follows. Peptide solubilized by being stirred into 40:60 = acetonitrile:water (both containing 0.1% TFA, v/v) at ≈60 °C was chromatographed using a Zorbax C-18 preparative column maintained at 60 °C and eluted from the column using a 50 min gradient from 25 to 65% (v/v) acetonitrile containing 0.1% (v/v) TFA. Purity was assessed by analytical RP-HPLC using a Vydac C-18 column. Mass of the product was verified using MALDI-TOF and ESI mass spectrometry.

Kinetics of Fibrillogenesis. The purified Aβ peptides were stored as follows. Peptide was dissolved at ≈50 °C into 30:70 acetonitrile:water containing 0.1% TFA (v/v) and lyophilized as aliquots of 0.5 mg in siliconized 1.5 mL tubes, and then it was stored at −20 °C. For fibrillogenesis assays, peptide concentration in buffer was assessed from absorbance at 274.6 nm, using the extinction coefficient for tyrosine of 1420 M^{-1} cm^{-1}. Fibrillogenesis was followed by thioflavin fluorescence at 37 °C. At various time points, 10 μL aliquots were taken, diluted into 1 mL of 10 μM Thioflavin T solution, in 10 mM sodium phosphate buffer, pH 7.40. The sample was pipetted vigorously, and fluorescence was monitored. Measurements (λ_{EX} = 446 nm, λ_{EM} = 490 nm) were made on a Hitachi F2000 fluorescence spectrophotometer and, after a 3 s delay, were averaged for 10 s with a bandwidth of 10 nm and a photomultiplier voltage of 700.

To compare the fibrillogenesis kinetics of $A\beta_{1-40}$-Lactam(D23/K28) with those of $A\beta_{1-40}$ we first compared a number of fibrillogenesis conditions for $A\beta_{1-40}$ to determine which gave the most reproducible kinetics, and most closely approximated "seed-free" conditions. A number of different techniques have been proposed for pretreating $A\beta_{1-40}$ peptides to ensure reproducibility of kinetics, where monomer is predominantly or exclusively present at the initiation of the reaction. We assessed multiple conditions, using various combinations of the following: (1) solvents to induce disaggregation (neat HFIP, neat DMSO, neat TFA, 1 mM NaOH); (2) sonication (varying time from 0 to 4 h); (3) removal of above solvents (by complete drying with N_2, or dilution to <2% final concentration); (4) buffers for resolubilizing disaggregated peptides (100 mM Tris, 10 mM sodium phosphate buffer, pH 7.40, with and without 150 mM NaCl, 5-fold diluted PBS); (5) temperature at which fibrils were grown (37 °C, room temperature); (6) agitation (stirring) or quiescence during fibril growth. One additional procedure evaluated was the isolation of a monomer population of peptide using size exclusion chromatography (Superdex 75, 10 mM sodium phosphate buffer, pH 7.40 or 10.00), followed by concentration of the peptide by Amicon filtration. Although the size exclusion procedure reproducibly yielded monomeric peptide, it was not feasible because no method could be found to concentrate the peptide to a level suitable for fibrillogenesis without inducing oligomerization and aggregation of the peptide.

To assess whether the peptide solutions treated by these procedures were monomeric or aggregated, we examined the samples by size exclusion chromatography using a Superdex 75 (Amersham) column equilibrated with 10 mM sodium phosphate buffer, pH 7.40. This column achieves separation of monomeric $A\beta_{1-40}$ from smaller and larger aggregates. The most consistent and reproducible results were achieved by solubilizing peptides in neat DMSO at ≈5.8 mM, and then diluting the peptide into 10 mM sodium phosphate buffer, pH 7.40, 0.02% sodium azide, to yield a final peptide concentration of ≈115 μM. As shown in Figure 9B, this yielded a single peak corresponding with the retention time for monomer $A\beta_{1-40}$. In addition, initial thioflavin readings of these solutions were at background levels, suggesting that the β-strand structure recognized by the thioflavin was not present. Hence, this solubilization procedure was followed for all the kinetic experiments discussed below. For chromatography of $A\beta_{1-40}$-Lactam(D23/K28) (Figure 9C), peptide was initially dissolved in DMSO and diluted to 1−5 μM in 10 mM sodium phosphate, pH 7.40, and a final DMSO concentration of 0.5% (v/v).

For fibril seeding assays (cross-seeding and self-seeding), seeds were made from stocks of fibrils in which the thioflavin fluorescence was no longer increasing, the endpoint of the reaction. To make seeds, slurries of fibrils were sonicated in a Branson model B-22-4 water bath sonicator for 10 min. The amounts of seed added was expressed as a weight percentage of the mass of monomeric $A\beta_{1-40}$ in solution, i.e., 2%, 5%, 7%, and 10%. Seeds were added to solutions of monomeric $A\beta_{1-40}$, freshly prepared as described above.

Electron Microscopy. Five microliter aliquots of fibril slurries of $A\beta_{1-40}$ or $A\beta_{1-40}$-Lactam(D23/K28) were applied to a glow-discharged, 1−400-mesh, carbon-coated support film, washed with water, and stained with 1% uranyl acetate for 30 s. Micrographs were recorded using a FEI Tecnai F30 electron microscope at magnifications of 15000× and 98000×. In addition, the CCD camera added a magnification of all images of 1.4×.

Congo Red Binding. To measure Congo Red binding, 3 μL of 0.1% (w/v) Congo Red (Sigma) was added to 1 mL of 10 mM sodium phosphate buffer, pH 7.40. The absorbance spectrum was measured from 400 to 600 nm. Then ≈30 μg of fibrillar $A\beta_{1-40}$ or $A\beta_{1-40}$-Lactam(D23/K28) was added to the Congo Red solution and incubated for 30 min at 22 °C. The absorbance spectrum was repeated. Pipetting the

sample vigorously or vortexing the sample after incubation did not alter readings.

Solid-State NMR. 1-^{13}C-Val18 labeled Aβ_{1-40}-Lactam-(D23/K28) was prepared for fibril growth as described above. Fibrils were then dialyzed against MilliQ water, using dialysis tubing with a molecular weight cutoff of 500. The fibrils were then centrifuged at 13200*g* for 30 min, supernatant was removed, and the pellet was lyophilized. After the labeled sample was loaded into a 3.2 mm magic-angle spinning (MAS) rotor, the sample mass was approximately 1 mg.

Frequency-selective rotational echo double resonance (fsREDOR) measurements (*34*, *35*) were carried out on an Aβ_{1-40} fibril sample with uniform ^{15}N and ^{13}C labeling of Asp23, Lys28, Gly29, Ile32, and Val36, prepared as previously described (*1*).

Solid-state NMR measurements were performed at 100.8 MHz ^{13}C NMR frequency, using a Varian Infinity-400 spectrometer and a Varian 3.2 mm MAS probe. All measurements were performed at room temperature. Frequency-selective ^{15}N−^{13}C fsREDOR data were acquired as described by Jaroniec et al. (*35*), with an MAS frequency of 9.0 kHz, selective ^{15}N and ^{13}C Gaussian π pulse lengths of 1.0 ms, hard ^{15}N π pulse lengths of 15 μs, and 110 kHz proton decoupling fields. In these measurements, selective π pulses are applied with the radio frequency carrier frequency at the ^{13}C and ^{15}N chemical shifts of C_γ of Asp23 and N_ϵ of Lys28, respectively, to select the magnetic dipole−dipole coupling between these nuclear spins while suppressing all other dipole−dipole couplings, scalar couplings, and inhomogeneous broadening (*35*). ^{13}C constant-time, finite-pulse radio frequency driven recoupling (fpRFDR-CT) data were acquired as previously described (*19*, *36*), with ^{13}C π pulse lengths of 15 μs in the fpRFDR periods, 20.0 kHz MAS, 110 kHz proton decoupling fields, and pulsed spin locking in the signal detection period to enhance sensitivity (*1*).

Simulations of fsREDOR data assumed a two-spin system and ideal radio frequency (rf) pulses (i.e., negligible effects of chemical shift anisotropy, rf inhomogeneity, and incomplete inversion by the selective π pulses). Simulations of fpRFDR-CT data used a six-spin system in a linear chain, with initial spin polarization on the central two spins to minimize end effects, and assumed an ideal rf pulse sequence (i.e., negligible effects of chemical shift anisotropy, rf inhomogeneity, and spin relaxation). Previous studies have validated the assumptions in these simulations (*19*, *35*).

RESULTS

Evidence of Asp23/Lys28 Salt Bridge from Solid-State NMR. To investigate whether there is a salt bridge between residues Asp23 and Lys28 in Aβ_{1-40}, fsREDOR experiments were carried out on Aβ_{1-40} fibrils, uniformly ^{15}N,^{13}C-labeled at Asp23, Lys28, Gly29, Ile32, and Val36. The fsREDOR technique was chosen for these experiments because it permits the measurement of distances between specific ^{13}C-labeled and ^{15}N-labeled sites in samples with multiple uniformly labeled residues (*35*) in this case between C_γ of Asp23 and N_ϵ of Lys28, and because Aβ_{1-40} fibril samples with multiple uniformly labeled residues had been prepared by Petkova et al. for measurements of ^{13}C and ^{15}N chemical shifts in two-dimensional solid-state NMR spectra (*1*). The

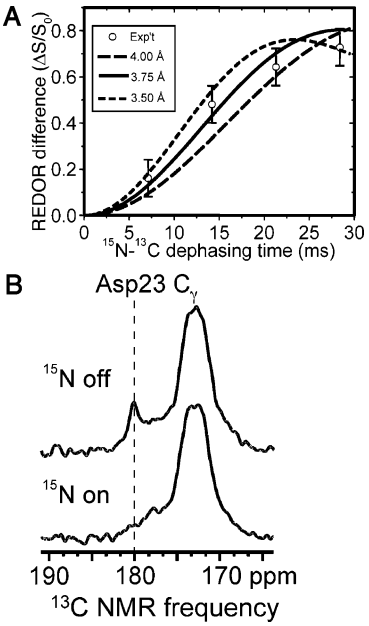

FIGURE 2: (A) Measurement of a ^{15}N−^{13}C nuclear magnetic dipole−dipole coupling between N_ϵ of Lys28 and C_γ of Asp23 in Aβ_{1-40} fibrils, using the frequency-selective REDOR solid-state NMR technique. Error bars are based on RMS noise in the NMR spectra. Simulations for several N_ϵ−C_γ distances are shown. These data indicate a distance of 3.8 ± 0.2 Å. (B) Portion of the ^{13}C MAS NMR spectrum, at 28.4 ms REDOR dephasing time. The Asp23 C_γ peak at 180 ppm is strongly reduced when a selective ^{15}N radio frequency pulse at the NMR frequency of the Lys28 N_ϵ is applied in the middle of the dephasing period. REDOR data are the difference between C_γ peak areas without and with the ^{15}N pulse (ΔS) divided by the peak area without the ^{15}N pulse (S_0). Signal centered at 172 ppm arises from carbonyl carbons of labeled Asp23, Lys28, Gly29, Ile32, and Val36 residues, which are not strongly coupled to the N_ϵ of Lys28.

results of these experiments are shown in Figure 2, along with simulated fsREDOR curves for a range of possible distances between C_γ of Asp23 and N_ϵ of Lys28. By comparing experimental and simulated data, we estimate a distance of 3.75 ± 0.25 Å, consistent with a salt bridge between the oppositely charged side chains. Restrained energy minimization to generate a molecular model consistent with the solid-state NMR data (*1*) indicates that these contacts are both intramolecular and intermolecular (to nearest neighbors in the β-sheet structure). Although not previously published, the data in Figure 2 were used in the development of the structural model in Figure 1 (*1*).

Rationale and Design of Aβ_{1-40}-Lactam(D23/K28) Peptide. The structure proposed for Aβ_{1-40} fibrils by Petkova et al. (*1*) contains a bend in the side-chain dimension, encompassing residues D^{23}VGSNKG^{29}, separating two in-register, parallel β-sheets. In contrast to typical β-turn structures, which are stabilized by torsional angle considerations (*37*−*39*) and, typically, a backbone hydrogen bond (e.g., between C═O of the *i*th residue and the N−H of the third residue in a type I β-turn), the bend structure here, between the β-sheets, appears to be stabilized by hydrophobic effects and also a salt bridge between Asp23 and Lys28. Although a β-turn in this region of the Aβ_{1-40} sequence was suggested in early studies of Aβ_{1-40} fibrils (*24*, *40*), a true β-turn is inconsistent with the later solid-state NMR data.

Kinetics of Aβ fibril formation typically show a lag period followed by the rapid accumulation of fibrillar products.

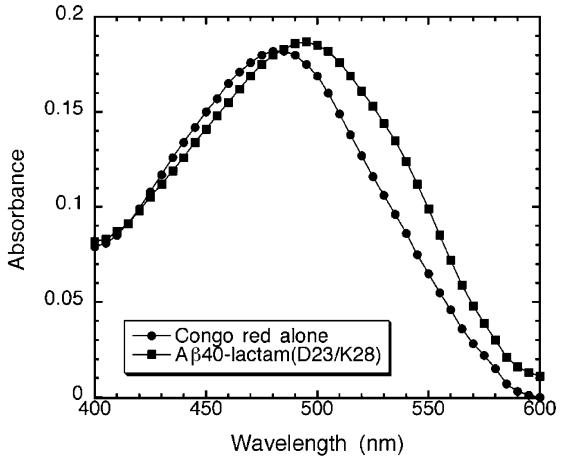

FIGURE 3: Congo Red absorption spectra from 400 to 600 nm. When $A\beta_{1-40}$-Lactam(D23/K28) fibrils are incubated with the Congo Red, the dye binds to the fibril and gives a red shift in absorbance typical of amyloid fibrils.

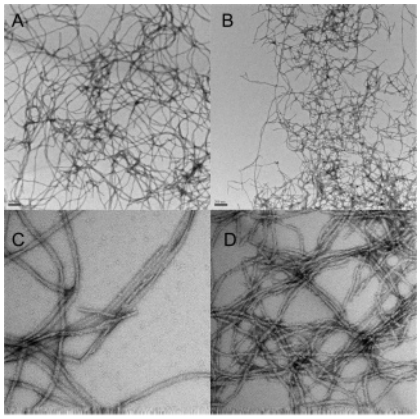

FIGURE 4: Electron micrographs of negatively stained fibrils formed by $A\beta_{1-40}$ (A, C, at 15000× and 98000× magnification, respectively), and $A\beta_{1-40}$-Lactam(D23/K28) (B, D, at 15000× and 98000× magnification, respectively). Fibrils were grown from ≈115 μM peptide in 10 mM sodium phosphate, pH 7.40 from a peptide stock in DMSO (final DMSO concentration <2%). $A\beta_{1-40}$ fibrils exhibit typical morphology of long, unbranched, twisting amyloid fibrils. $A\beta_{1-40}$-Lactam(D23/K28) are not as frequently twisted and are composed of single fibrils.

While this pattern has been attributed to the slow formation of a "seed" or "nucleus", it is also clear that fibrillogenesis must include one or more conformational changes, since fibrillar Aβ has a high β-sheet content, while monomeric Aβ is essentially unstructured (*24, 26*). We hypothesized that a conformational change (including formation of β-sheet structure) and oligomerization is a slow, perhaps even rate-limiting step in $A\beta_{1-40}$ fibril formation. If this hypothesis were correct, then a congener of $A\beta_{1-40}$ that bypassed the need for this conformational change should form fibrils without a lag period, and yet the fibrils should still closely resemble those formed by $A\beta_{1-40}$.

The fsREDOR data presented above suggested a convenient way to produce such a conformationally restricted congener of $A\beta_{1-40}$. If the salt bridge between Asp23 and Lys28 that flanks this bend region were mostly intramolecular rather than intermolecular, then an amide bond between the β-carboxyl group of the Asp and the ε-amine group of the Lys, creating a lactam bridge within a single peptide, would mimic such an interaction.

We synthesized $A\beta_{1-40}$-Lactam(D23/K28), with the sequence

$$NH_2\text{-DAEFRHDSGY}^{10}\text{EVHHQKLVFF}^{20}\text{-}$$
$$\text{AEDVGSNKSA}^{30}\text{IIGLMVGGVV}^{40}\text{-COOH}$$

where the tie bar represents the lactam cross-link. Details of the synthesis are described in Experimental Procedures. Low yields of this peptide are attributable to the high propensity of the peptide to aggregate.

Demonstration that $A\beta_{1-40}$-Lactam(D23/K28) Fibrils Have Structure Similar to That of $A\beta_{1-40}$ Fibrils. $A\beta_{1-40}$-Lactam(D23/K28) rapidly formed fibrils under several solvent conditions. For example, 230 μM peptide formed fibrils within an hour at 37 °C, in 100 mM Tris buffer, 150 mM NaCl, pH 7.40. The aggregates were thioflavin T positive to a level similar to but consistently slightly lower than that observed for $A\beta_{1-40}$ at the same concentration. To confirm that these were typical amyloid fibrils, a Congo Red binding assay was performed. Figure 3 demonstrates that the $A\beta_{1-40}$-Lactam(D23/K28) fibrils bind Congo Red, displaying a characteristic red shift in absorbance for amyloid fibrils. The fibrillar nature of these aggregates was also documented by electron microscopy (Figure 4). The EM images indicate that fibrils formed by $A\beta_{1-40}$-Lactam(D23/K28) and $A\beta_{1-40}$ are similar in length. These data indicate that the $A\beta_{1-40}$-Lactam(D23/K28) aggregate is indeed fibrillar.

The morphology of the fibrils made by $A\beta_{1-40}$ and $A\beta_{1-40}$-Lactam(D23/K28) peptides are similar but not identical, even though they were grown under identical conditions. Only infrequent $A\beta_{1-40}$-Lactam(D23/K28) fibrils have the appearance of a twisting duplex, an appearance seen more frequently in samples of $A\beta_{1-40}$ fibrils. In addition, the diameter (± standard deviation) of the $A\beta_{1-40}$-Lactam(D23/K28) fibrils is somewhat smaller than that of $A\beta_{1-40}$ fibrils, i.e., 10.88 ± 1.5 nm for $A\beta_{1-40}$ and 7.34 ± 0.85 nm for $A\beta_{1-40}$-Lactam(D23/K28) fibrils.

Solid-State NMR of $A\beta_{1-40}$-Lactam(D23/K28). To test the structural similarity of $A\beta_{1-40}$ and $A\beta_{1-40}$-Lactam(D23/K28) fibrils at the molecular level, we used solid-state NMR. Figure 5A shows the one-dimensional (1D) ^{13}C MAS NMR spectrum of $A\beta_{1-40}$-Lactam(D23/K28) containing 1-^{13}C-Val18. Carbonyl ^{13}C chemical shifts are sensitive to secondary structure (*41*). The peak at 171.7 ppm for the labeled site is typical for a β-strand conformation (i.e., 2.9 ppm upfield shift from the random coil value (*42*)), and is similar to the chemical shift of Val18 (171.0 ppm) reported for uncross-linked $A\beta_{1-40}$ fibrils that exhibit the salt bridge between Asp23 and Lys28 (*43*). Although the difference between Val18 carbonyl chemical shifts in $A\beta_{1-40}$ and $A\beta_{1-40}$-Lactam(D23/K28) fibrils is real, the small magnitude of this difference (e.g., relative to the solid-state NMR line widths) suggests that the underlying structural differences are minor. Small differences in backbone torsion angles around Val18 would be sufficient to account for the differences in carbonyl chemical shifts. The ^{13}C NMR line width of 2.7 ppm is similar to carbonyl line widths observed in $A\beta_{1-40}$ fibrils (*1, 19*). Significantly larger line widths are observed in unstructured peptides (6−8 ppm) (*44*).

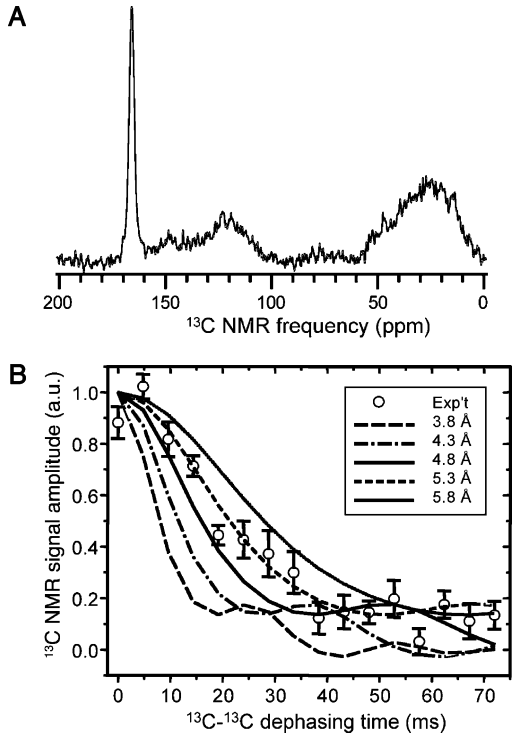

FIGURE 5: (A) ^{13}C NMR spectrum of Aβ_{1-40}-Lactam(D23/K28) fibril sample with a ^{13}C-carbonyl label on Val18 (peak at 171.7 ppm relative to tetramethylsilane, 2.7 ppm line width), obtained at 100.8 MHz NMR frequency with 20.0 kHz MAS. The deviation from a random coil chemical shift of 174.6 supports a β-strand conformation at Val18. Broad peaks centered at 25 and 120 ppm are primarily probe background signals. Spectrum was acquired in 40960 scans, with approximately 1 mg of fibrils. (B) Experimental ^{13}C fpRFDR-CT data for the same sample, acquired at 100.8 MHz NMR frequency with 20.0 kHz MAS, 6400 scans per data point, and pulsed spin locking to enhance sensitivity. Error bars are based on RMS noise in the NMR spectra. Data are corrected for natural-abundance ^{13}C signal contributions as described in ref *19*. Simulated curves are for a linear chain of ^{13}C spins with indicated spacings. These data indicate nearest-neighbor intermolecular distances of 5.0 ± 0.3 Å for Val18 carbonyl carbons, consistent with an in-register, parallel β-sheet structure.

To investigate supramolecular structure, the fpRFDR-CT technique (*19, 36*) was used to measure intermolecular distances between Val18 carbonyl carbons in Aβ_{1-40}-Lactam-(D23/K28) fibrils. The fpRFDR-CT data for Aβ_{1-40}-Lactam-(D23/K28) fibrils (Figure 5B) containing the Val18 carbonyl label are nearly identical to data for Aβ_{1-40} fibrils (*19*), indicating a nearest-neighbor intermolecular distance between Val18 carbonyl sites of approximately 5.0 ± 0.3 Å. This distance is consistent with an in-register, parallel β-sheet structure, where distances of 4.7 ± 0.1 Å are expected. The fpRFDR-CT data could also be consistent with an out-of-register parallel β-sheet structure with a one-residue shift in backbone hydrogen bond registry, where nearest-neighbor intermolecular distances in the 5.0−5.5 Å range are expected. On the basis of an examination of energy-minimized parallel β-sheet models, larger shifts in backbone hydrogen bond registry would produce nearest-neighbor intermolecular distances greater than 6.5 Å and can be ruled out. Antiparallel β-sheet structures, which to date have only been observed experimentally in amyloid fibrils when the component peptides comprise fewer than 20 residues and contain a single β-strand and a single hydrophobic segment (*45*−*48*), are inconsistent with the fpRFDR-CT data unless Val18 is hydrogen bonded to either Val18 or Phe19 (i.e., residue *i* hydrogen-bonds to either residue 36-*i* or 37-*i* in an antiparallel alignment of neighboring peptide chains). Otherwise, nearest-neighbor intermolecular distances for the Val18 carbonyl would exceed 6.0 Å.

Fibrillogenesis Kinetics. Aβ_{1-40} fibrillogenesis exhibited a lag period of 3000 min. Fibril growth appeared to be complete at ≈15000 min. In contrast, under the same conditions, Aβ_{1-40}-Lactam(D23/K28) initiated fibril growth immediately and exhibited no lag phase, completing fibrillogenesis in ≈30 min. Presence of fibrils was confirmed by electron microscopy. To compare the fibrillogenesis kinetics of Aβ_{1-40} and Aβ_{1-40}-Lactam(D23/K28), the kinetic data were treated as follows. For Aβ_{1-40}-Lactam(D23/K28), data could be fit straightforwardly to a monoexponential equation, as shown in Figure 6A (solid line). In the case of Aβ_{1-40} however, where there was a lag period, the kinetics of fibrillogenesis could not be fitted to a monoexponential equation, nor to other common kinetic rate equations (e.g., sequential or parallel first-order equations, second-order equation). Instead, we observed that the data fitted the equation of a "stretched exponential", as is often observed for complex kinetic schemes (e.g., Pasternack et al. (*49*)). In this analysis, the free monomer concentration decreases exponentially as a power of time, i.e.,

$$([M] - [M]_\infty) = ([M_0] - [M]_\infty) \exp(-(kt)^n) \quad (1)$$

where [M] is the free monomer concentration at time *t*, $[M]_0$ is the initial total peptide concentration, and $[M]_\infty$ is the concentration of free monomer units at equilibrium. (Aβ40 is monomeric by size exclusion chromatography and sedimentation equilibrium analytical ultracentrifugation under conditions used for these assays. It is not possible to exclude the presence of a small amount of dimeric peptide under these circumstances, however.) Leyvraz et al. (*50*) define the parameter *n* as a power function of time, which they use to describe kinetics of fractal growth. Since the total peptide concentration is the sum of monomer and aggregates, i.e., $[M_0] = [M] + [Agg]$, it follows that

$$[Agg] = ([M_0] - [M]_\infty)\{1 - \exp(-(kt)^n)\} \quad (2)$$

We followed the formation of fibrillar aggregates of Aβ_{1-40} by thioflavin fluorescence, which yields the following equation:

$$ThT = ThT_0 + \{(ThT_\infty - ThT_0)[1 - \exp(-(kt)^n)]\} \quad (3)$$

where ThT, ThT_0, and ThT_∞ represent thioflavin fluorescence readings at various times, at time = 0, and at infinite time, respectively.

The results of this analysis are shown in Figure 6A and Figure 6B, for Aβ_{1-40}-Lactam(D23/K28) and Aβ_{1-40}, respectively. From this analysis, we found that Aβ_{1-40}-Lactam-(D23/K28) formed fibrils with a rate, $k = 0.107$ min^{-1}, while for Aβ_{1-40}, $k = 1.07 \times 10^{-4}$ min^{-1}. That is, the rate of fibril formation by Aβ_{1-40}-Lactam(D23/K28) was 1000-fold greater than that of Aβ_{1-40}, at the same peptide concentration and under similar conditions. Therefore, the Aβ_{1-40}-Lactam-

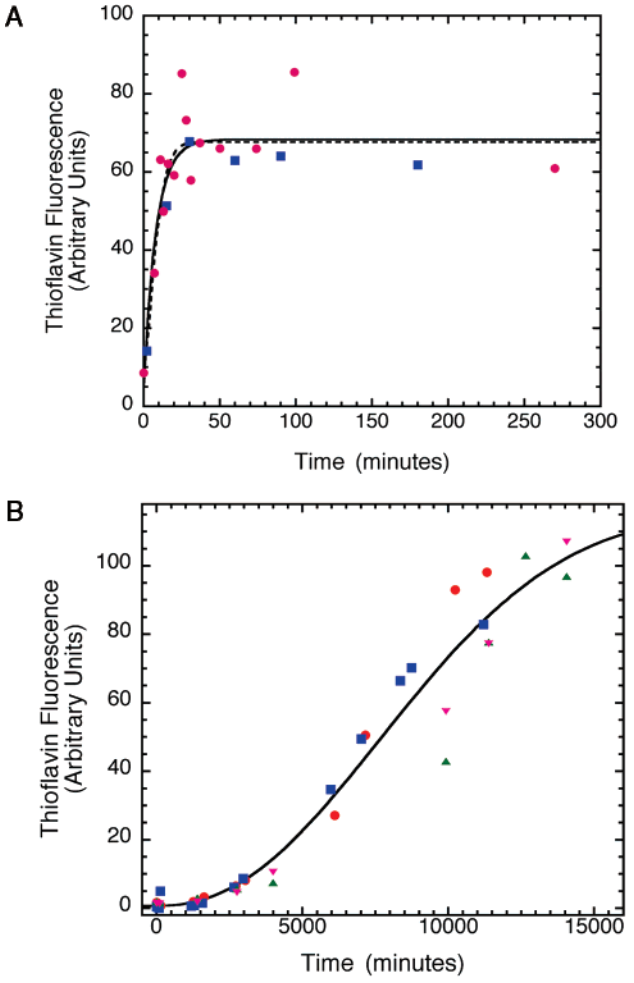

FIGURE 6: Fibril kinetic growth curves for Aβ_{1-40}-Lactam(D23/K28) (A) and Aβ_{1-40} (B) as a function of relative thioflavin T fluorescence. Peptide samples were incubated at 37 °C in 10 mM sodium phosphate, pH 7.40. Ten microliter samples were removed at various times to measure thioflavin T fluorescence. Curves are calculated on the basis of representative data (various symbols) from two (panel A) and four (panel B) experiments, and normalized to a maximum fluorescence of 100. Growth of Aβ_{1-40} is a typical sigmoidal growth curve with a lag phase of ≈3000 min (≈2.5 days). In the figure, lines represent theoretical curves derived from nonlinear least-squares fit of the data. For Aβ_{1-40}, data were fitted to the equation $ThT = ThT_0 + \{(ThT_\infty - ThT_0)[1 - \exp(-(kt)^n)]\}$, where ThT, ThT_0, and ThT_∞ represent thioflavin fluorescence readings at various times, at time = 0, and at infinite time, respectively. For Aβ_{1-40}-Lactam(D23/K28), fibrillogenesis showed essentially no lag phase, with fibril growth completed at ≈30 min. When fibrillogenesis data for Aβ_{1-40}-Lactam(D23/K28) were analyzed by this equation, the results were essentially identical to those obtained when the data results were analyzed using the equation of first-order kinetics, i.e., $ThT = ThT_0 + (ThT_\infty - ThT_0)[1 - \exp(-kt)]$; these theoretical curves are shown as dashed and solid lines, respectively.

(D23/K28) demonstrates greatly accelerated incorporation into amyloid fibrils.

One additional feature of this kinetic analysis comes from the calculation of the parameter n. While for Aβ_{1-40}, $n = 2.24 \pm 0.37$, for Aβ_{1-40}-Lactam(D23/K28), $n = 1.46 \pm 0.64$, i.e., indistinguishable from unity, within the limits of experimental error. The theoretical curve for Aβ_{1-40}-Lactam(D23/K28) fibrillogenesis kinetics as analyzed by eq 3 is the dotted line in Figure 6A. This curve is not distinguishable from that of monoexponential kinetics, i.e. (solid line in Figure 6A),

$$ThT = ThT_0 + (ThT_\infty - ThT_0)[1 - \exp(-kt)] \quad (4)$$

Equation 4 yielded $k = 0.122 \pm 0.029$ min^{-1}, the same, within experimental error, as the value obtained using eq 3.

In addition, this analysis provided a convenient way to approximate the length of the lag period: values for the parameters obtained using eq 3 were then used to derive a value for the midpoint in the rise in thioflavin fluorescence (in Figure 6B, the midpoint occurred at $t = 8.52 \times 10^3$ min). From the calculated local slope at this midpoint, we then estimated the lag period as the x-intercept of the line formed tangent to the midpoint of the theoretical curve. Using this procedure, we estimated that the lag period for Aβ_{1-40} fibril formation was 3.06×10^3 min (≈2.5 days). A similar calculation for Aβ_{1-40}-Lactam(D23/K28) yields a lag period of ≈0.12 min., i.e., essentially no lag period.

Seeding of Aβ_{1-40} Fibril Growth by Addition of Aβ_{1-40} or Aβ_{1-40}-Lactam(D23/K28) Fibrils. An additional criterion for the similarity between the Aβ_{1-40} and Aβ_{1-40}-Lactam(D23/K28) fibrils is that the fibrils of one should be able to nucleate and thus accelerate growth of fibrils by solutions of the other peptide. The efficiency by which self or other proteins seed amyloid growth has been shown to be related to structural similarity, including sequence similarity (*51*), though the correlation between seeding efficiency and primary structural homology is imperfect (*52*). Accordingly, we examined whether addition of Aβ_{1-40}-Lactam(D23/K28) fibrils stimulates the growth of monomeric Aβ_{1-40} into fibrils of specific morphology. The reverse experiment cannot be performed because polymerization of Aβ_{1-40}-Lactam(D23/K28) is virtually instantaneous with no lag phase, even under conditions intended to slow fibrillogenesis; e.g., temperature = 4 °C, the addition of glycerol to increase viscosity, and lower peptide concentrations (25 μM). We also examined the acceleration of Aβ_{1-40} fibril growth when Aβ_{1-40} fibril seeds were added to solutions of monomeric Aβ_{1-40}.

As expected, the addition of Aβ_{1-40} fibrils accelerated fibril growth of a solution of 100 μM monomeric Aβ_{1-40} (Figure 7A). Aβ_{1-40}-Lactam(D23/K28) fibrils also accelerated fibril growth of solutions of monomeric Aβ_{1-40} (Figure 7B) and eliminated the lag phase. The kinetics were analyzed as monoexponential as described above, because the experimental data indicated the absence of a detectable lag phase. In both experiments, rate constants for fibril growth appeared to increase proportionately with the amount of fibril seed added (expressed as weight percent of the mass of Aβ_{1-40} in solution). Electron micrographs of Aβ_{1-40} seeded with either Aβ_{1-40} (Figure 8A) or Aβ_{1-40}-Lactam(D23/K28) seed (Figure 8B) were analyzed for fibril diameter as described above. The mean diameters (± standard deviation) were 11.2 ± 1.5 nm and 10.1 ± 1.4 nm, respectively. Within experimental limits, these numbers are not different, and also are the same as the diameter of Aβ_{1-40} fibrils grown under unseeded conditions (10.7 ± 1.4 nm). In addition, the Aβ_{1-40} fibrils grown using either seed were indistinguishable morphologically from Aβ_{1-40} fibrils grown under unseeded conditions.

Soluble Oligomers of Aβ_{1-40}-Lactam(D23/K28) at 1−5 μM Concentrations. Aβ_{1-40} peptide used for fibrillogenesis assays was entirely monomeric (i.e., undetectable oligomer) by size exclusion chromatography using Superdex-75. When lyophilized Aβ_{1-40} was dissolved in DMSO, and the peptide

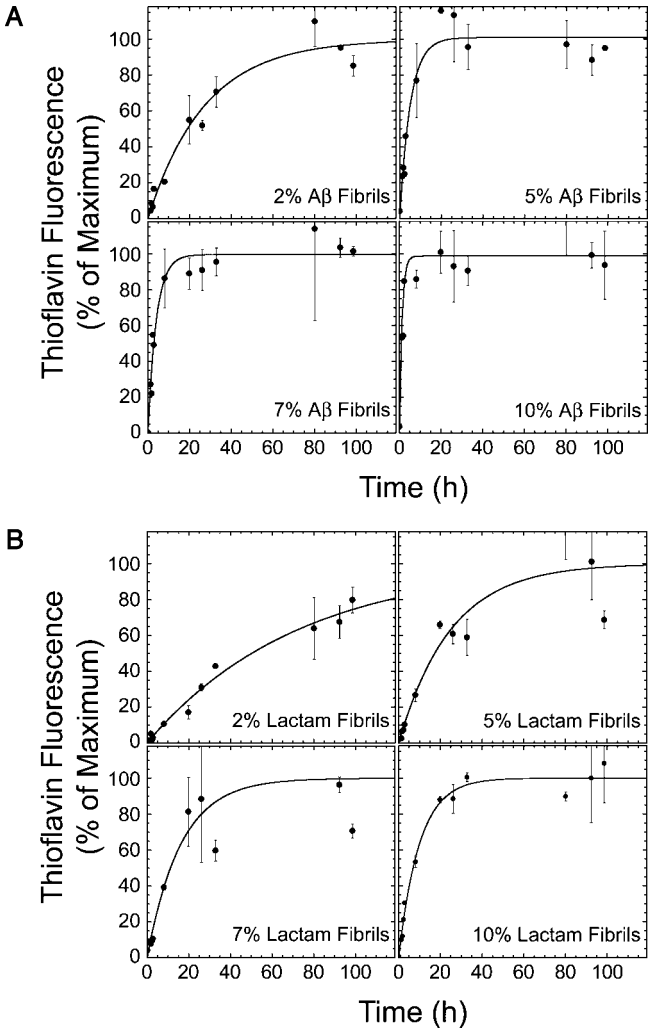

FIGURE 7: Aβ_{1-40}-Lactam(D23/K28) and Aβ_{1-40} fibrils "seeds" accelerate fibrillogenesis of Aβ_{1-40} solutions and eliminate the lag phase of fibrillogenesis. (A) Aβ_{1-40} fibrils expressed as weight fraction of the mass of 115 μM Aβ_{1-40} in solution were added to a solution of monomeric Aβ_{1-40}. Lines represent nonlinear least-squares fit of the data to a monoexponential growth function. (B) Aβ_{1-40}-Lactam(D23/K28) fibrils (expressed as weight fraction of the mass of 115 μM Aβ_{1-40} in solution) also accelerated fibril growth of solutions of monomeric Aβ_{1-40}, and also eliminated the lag phase. Data were fitted to a monoexponential growth curve.

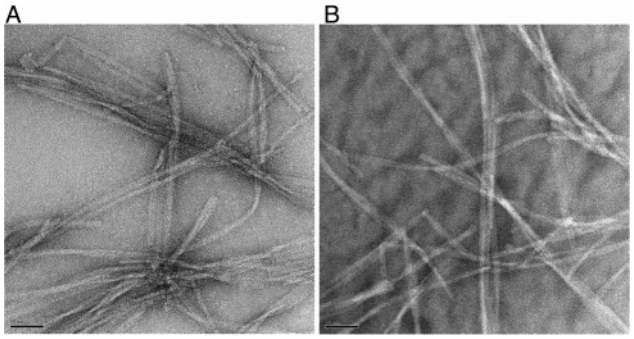

FIGURE 8: Electron micrographs of Aβ_{1-40} fibrils, grown using either 2% (mass/mass) Aβ_{1-40} fibril seeds (A) or 2% (mass/mass) Aβ_{1-40}-Lactam(D23/K28) fibril seeds. In addition, similar images were obtained of Aβ_{1-40} fibrils grown using 5%, 7%, or 10% Aβ_{1-40} or Aβ_{1-40}-Lactam(D23/K28) fibril seeds. Images show 98000× magnification.

diluted with 10 mM sodium phosphate, pH 7.40 to a final peptide concentration of ≈115 μM (final DMSO concentration < 2% (v/v)), the chromatogram showed predominantly or exclusively monomeric Aβ_{1-40} (Figure 9B). When Aβ_{1-40} was similarly treated using HFIP in lieu of DMSO, however,

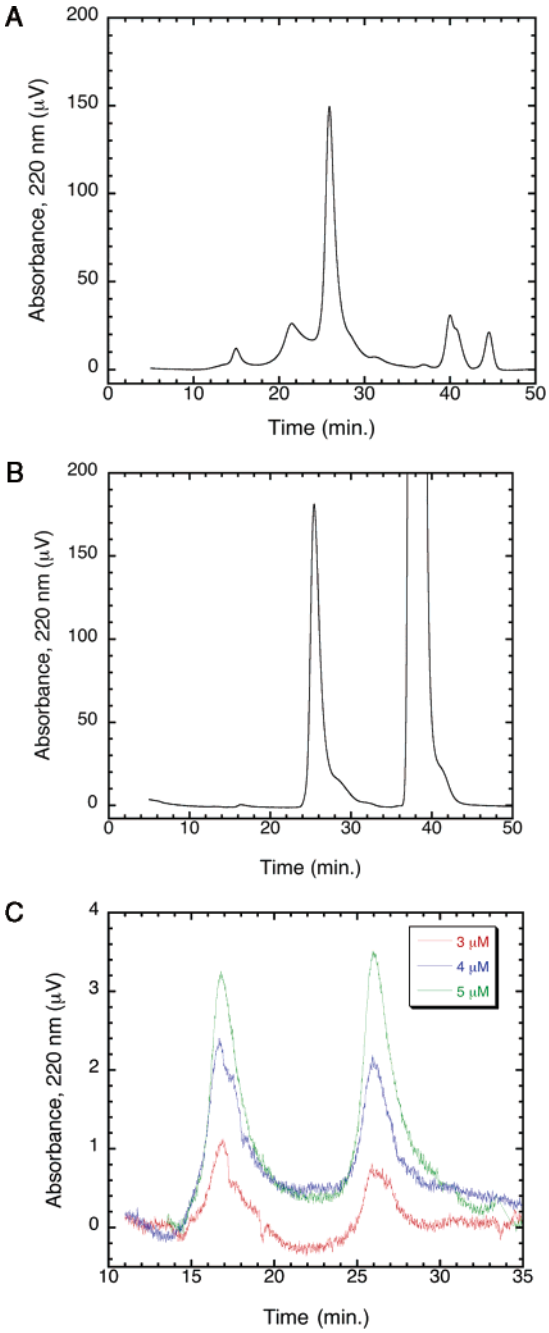

FIGURE 9: Size exclusion chromatography of Aβ peptides using Superdex-75. (A) In this sample, Aβ_{1-40} was treated with HFIP and dissolved in 0.2X PBS, pH 7.40. Peaks representing monomeric and various forms of oligomeric soluble Aβ_{1-40} are shown in the figure. (B) A sample of purified and lyophilized Aβ_{1-40} was re-solubilized in 40% acetonitrile in water (both containing 0.1% TFA, v/v) and then aliquoted and lyophilized in siliconized tubes. The lyophilized powder was dissolved in DMSO and then transferred into 10 mM sodium phosphate, pH 7.40 as described in Experimental Procedures, so that the final peptide concentration was ≈115 μM, and the DMSO concentration was <2% (v/v). The chromatogram shows only monomeric Aβ_{1-40}, i.e., any oligomers, if present, were below the limits of detection. (C) A sample of Aβ_{1-40}-Lactam-(D23/K28), prepared as described in Experimental Procedures. Even at ≈1 μM, the solution of Aβ_{1-40}-Lactam(D23/K28) gave a chromatogram that indicated the presence of both monomers and small oligomers.

peaks of monomer and various oligomers were present (Figure 9A).

In contrast to Aβ_{1-40}, solutions of Aβ_{1-40}-Lactam(D23/K28), prepared by first dissolving it in DMSO or HFIP, contained soluble oligomer at all peptide concentrations tested. This soluble oligomer was always present, even when Aβ_{1-40}-Lactam(D23/K28) concentration was as low as 1 μM (Figure 9C). Aβ_{1-40} oligomers display "micelle-like" behavior, as shown by DPH fluorescence measurements. For Aβ_{1-40} prepared as described above, DPH fluorescence measurements indicated CMC $\approx$40$-$50 μM. Similar measurements for Aβ_{1-40}-Lactam(D23/K28) yielded a CMC of $\approx$1$-$3 μM (data not shown).

These data, taken with the lack of a detectable lag period in fibrillogenesis kinetics, suggest that Aβ_{1-40}-Lactam(D23/K28) bypasses a rate-limiting step in fibril formation. Oligomers of the peptide may serve as nucleation sites that allow essentially immediate fibril growth.

DISCUSSION

Solid-state NMR has advanced our understanding of amyloid structure and has led to the generation of an explicit, though not fully experimentally determined structural model of the Aβ_{1-40} fibril. In this paper, we have described a model peptide based on the structure proposed from solid-state NMR and other data for Aβ_{1-40} fibrils. Aβ_{1-40}-Lactam(D23/K28) contains a lactam bridge between the side chains of Asp23 and Lys28, which resembles an intramolecular salt bridge between these residues in a "bend" region of Aβ_{1-40} fibrils.

Since soluble, monomeric Aβ_{1-40} is largely unstructured (*26*), association of this peptide into an oligomer/nucleating seed, and then fibrils presumably entails conformational changes, including formation of β-sheets and the bend structure. We hypothesized that formation of this bend might be a rate-limiting step in fibril formation, contributing to the lag period typically observed in the kinetics of Aβ_{1-40} fibrillogenesis. From this hypothesis, one would predict that the lactam peptide could bypass this unfavorable step, eliminating a lag period in fibril growth, because of its stable preformed bend.

Previous investigators reported constraining the structure of Aβ peptides using lactam bridges. For example, Esler et al. (*53*) examined a congener of Aβ_{10-35} cyclized between H14K and E22. Similarly, Kapurniotu et al. (*54*) studied an Aβ_{1-28} congener, cyclized between L17K and A21D. In both cases, these peptides were not able to form amyloid, possibly because the lactam bridge disrupted one of the β-sheet segments, rather than forming a structure like the "bend" in the Aβ_{1-40} fibril model. These two lactam bridged peptides suggest that bends and related non-β-sheet structures need to be in a specific and correct location for fibril propagation.

Aβ_{1-40}-Lactam(D23/K28) has a high propensity to aggregate into fibrils. The fibrillar product of Aβ_{1-40}-Lactam(D23/K28) is similar in structure to fibrils of the un-cross-linked Aβ_{1-40} as evidenced by ThT fluorescence, Congo Red binding, electron microscopy, and the solid-state NMR data presented above. Small differences exist between fibrils formed from Aβ_{1-40} as compared with those formed by Aβ_{1-40}-Lactam(D23/K28). The former have a larger diameter than the latter (10.88 $\pm$ 1.5 nm and 7.34 $\pm$ 0.85 nm, respectively) and show slightly higher thioflavin fluorescence. The electron microscopic differences between Aβ_{1-40} and Aβ_{1-40}-Lactam(D23/K28) may reflect differences in molecular organization, e.g., whether the salt bridge between Asp23 and Lys28 is intramolecular or intermolecular. These differences notwithstanding, the most notable feature of Aβ_{1-40}-Lactam(D23/K28) is that its fibrillogenesis kinetics do not show a detectable lag period. In contrast, fibrillogenesis of Aβ_{1-40} shows sigmoidal kinetics, which we analyzed using the equation of a "stretched exponential". We calculated a rate constant for Aβ_{1-40}-Lactam(D23/K28) fibrillogenesis that was $\approx$1000-fold greater than for Aβ_{1-40}. Aβ_{1-40}-Lactam(D23/K28) fibrillogenesis also fitted well to the stretched-exponential equation, but the scaling parameter, *n*, was close to unity, so the kinetics could not be distinguished from monoexponential kinetics within experimental error. Using the latter equation, the lag period is calculated as 0.12 min, i.e., essentially no lag period. These data indicate that Aβ_{1-40}-Lactam(D23/K28), which has the same amino acid sequence as Aβ_{1-40}, can bypass a kinetic barrier to fibril formation. The size exclusion chromatography data and DPH fluorescence data show that Aβ_{1-40}-Lactam(D23/K28) forms micelle-like aggregates even at concentrations $\approx$1 μM, indicating that this peptide models a conformation that is highly favorable for nucleation of amyloid fibrils.

As a largely unstructured molecule in solution, Aβ_{1-40} can sample multiple conformational states. As a result of the conformational plasticity of Aβ_{1-40}, more than one of its solution phase conformations could be "fibril competent", while others may be nonfibrillogenic or may form fibrils with slower kinetics (for example, variations in the alignment of the β-sheet (*55*, *56*)). There has been evidence of structural heterogeneity in the Aβ_{1-40} fibrils based on fibril growth conditions, which has indeed been observed in solid-state NMR measurement (*1*, *43*, *57*); for example, fibrils formed under "quiescent" conditions differ structurally from those formed in stirred ("agitated") solutions (*43*). Aβ_{1-40}-Lactam(D23/K28) is effectively "locked" into one or a small number of particular fibrillogenic structures induced by the lactam bond in the bend region. Fibrils formed from this peptide may be capable of adopting some but not all of the possible conformations of Aβ_{1-40} in solution and therefore might be predicted to form a less heterogeneous set of structures of any given growth conditions. If Aβ_{1-40}-Lactam(D23/K28) preferentially adopts a "fibril competent", micelle-like, aggregated structure, then the conformational constraint makes this structure readily available in solution, and nucleation followed by polymerization proceeds at a faster rate.

Aβ_{1-40}-Lactam(D23/K28) is also quite effective at cross-seeding, as shown by the ratio of $k_{\text{cross-seed}}/k_{\text{self-seed}}$. For example, this ratio was 0.38 for $\approx$2% (w/w) Aβ_{1-40}-Lactam(D23/K28) seeding fibril growth from Aβ_{1-40} solutions. The slightly lower effectiveness of Aβ_{1-40}-Lactam(D23/K28) to seed Aβ_{1-40} as compared to self-seeding of Aβ_{1-40} could be explained by the slight variance in number of growth sites with the added fibril seed, or nonidentical fibril growth sites between the two fibril seeds; these two explanations cannot be distinguished by the above experiments. Despite differences in experimental conditions, the level of cross-seeding that we observed can be compared with results obtained by O'Nuallain et al. (*52*), who studied seeding specificity in

amyloid growth induced by heterologous fibrils. The most efficient cross-seeding found by these authors was with islet amyloid polypeptide (IAPP) used as the seed aggregate. In a fibril elongation assay, IAPP seeds were 1.1% as efficient at promoting fibril elongation by $A\beta_{1-40}$ solutions as were $A\beta_{1-40}$ fibrils, i.e., comparable to $k_{cross-seed}/k_{self-seed} \approx 0.0011$. As a possibly more relevant comparison, we reanalyzed the data appearing in another study (*58*), in which $A\beta_{1-42}$ fibrils were used to cross-seed soluble $A\beta_{1-40}$. Using eq 3 and the data of their Figures 4 and 5, we calculated $k_{cross-seed}/k_{self-seed} \approx 0.033$ (for 10 μg/mL fibrillar $A\beta_{1-42}$ seeding a solution of 50 μM $A\beta_{1-40}$) and 0.0065 (for 20 μg/mL fibrillar $A\beta_{1-42}$ seeding a solution of 50 μM $A\beta_{1-40}$). Thus, $A\beta_{1-40}$-Lactam(D23/K28) is much more effective at cross-seeding $A\beta_{1-40}$ than even $A\beta_{1-42}$, which underscores the conformational similarity between $A\beta_{1-40}$ and $A\beta_{1-40}$-Lactam(D23/K28) fibrils. Electron micrographs of $A\beta_{1-40}$ fibrils grown using either $A\beta_{1-40}$ or $A\beta_{1-40}$-Lactam(D23/K28) seeds yielded fibrils of ≈10.5 nm diameter, i.e., the same as $A\beta_{1-40}$ fibrils grown under unseeded conditions. This suggests that the growth sites of the two seeds are virtually the same. We infer that the narrower fibrils arising in unseeded growth of $A\beta_{1-40}$-Lactam(D23/K28) result from the constraint of the peptide by the lactam cross-link, whereas growth of $A\beta_{1-40}$ fibrils on either seed is not subject to such constraints. At present, there is not sufficient data to explain the difference in diameters.

Why would formation of the bend structure and its salt bridge represent a kinetic barrier to fibril formation, and how does the lactam bond in $A\beta_{1-40}$-Lactam(D23/K28) overcome this barrier? Our results are consistent with the idea that hydrophobic effect, i.e., the clustering of hydrophobic side chains that shields them from water, drives formation of the bend structure. Whether this conformational change occurs in solution as a monomer, driving oligomer formation, or only after the peptide has oligomerized is not known. First, in the fibril structure proposed by Petkova et al. (*1*), the interior of the β-sheet duplex in an individual peptide buries many of the hydrophobic amino acid side chains. To cluster these hydrophobic residues requires that the salt bridge be formed, and in forming the salt bridge, it is necessary to desolvate the charged amino acids to some extent. We propose that the need to bury Asp23 and Lys28 in a dehydrated environment could represent a kinetic barrier to $A\beta_{1-40}$ fibril formation—a kinetic barrier that the lactam bond eliminates, mimicking an intramolecular salt bridge. Burial of Lys28 in the fibrils is suggested by solid-state NMR data (*1*) and by the fact that Lys28 is more protected against alkylation than either Lys16 or the α-amino group in fibrillar $A\beta_{1-40}$, even though all three amino groups are equally susceptible to alkylation in monomeric $A\beta_{1-40}$ (*59*). It is not possible without further experiments to say which of the above two factors—the decrease in the entropy of the unfolded state or eliminating the need to desolvate two charged residues—is more important.

The $A\beta_{1-40}$-Lactam(D23/K28) peptide overcomes an entropic penalty by restraining the two clusters of hydrophobic amino acids to lie in a pocket in apposition to one another, i.e., the lactam constraint decreases the entropy of the monomeric (nonfibrillar) state. In forming $A\beta_{1-40}$ fibrils of the structure shown in Figure 1, one would expect an energetic penalty of burying charged side chains in the dehydrated center formed by the side chains of hydrophobic amino acids of the two β-sheets. Some or all of this penalty, however, would be recovered by formation of a salt bridge between the side chains. Thus, forming the salt bridge could represent a kinetic, though not necessarily a thermodynamic, hindrance to fibril formation. In $A\beta_{1-40}$-Lactam(D23/K28), Asp23 and Lys28 are constrained to lie in a "buried" position, and the charges of these side chains are also neutralized, so that there is no such energetic penalty for placing them in the hydrophobic environment.

Clearly, amyloid formation from other peptides or proteins need not include a bend conformation of the type described for $A\beta_{1-40}$. Short peptides such as $A\beta_{16-20}$ form typical amyloid fibrils (*47*, *48*, *60*), and it is unlikely that formation of these fibrils requires the formation of a "bend" such as that discussed in this paper. Similarly, it is not known whether fibrils containing the salt bridge are more or less stable than fibrils containing blocked or "neutralized" modifications of Asp23 and Lys28 or substitutions of uncharged amino acids at these positions. In the case of $A\beta_{1-40}$, however, burial of the oppositely charged amino acids and the formation of a salt bridge in an apolar environment might represent a significant kinetic barrier to fibril formation of $A\beta_{1-40}$. Formation of the bend structure proposed as a conformational change during the lag phase may increase the ability of $A\beta_{1-40}$ to nucleate for fibril growth.

ACKNOWLEDGMENT

Some of the peptide purifications were performed by Hélène Miller-Auer, at The University of Chicago. The electron microscopy was performed in the laboratory of Dr. Robert Josephs at The University of Chicago. ESI-MS was performed by Dr. Giridher Reddy, and MALDI-TOF-MS was performed in the laboratory of Chang-Jin Qin, both at The University of Chicago.

REFERENCES

1. Petkova, A. T., Ishii, Y., Balbach, J. J., Antzutkin, O. N., Leapman, R. D., Delaglio, F., and Tycko, R. (2002) A structural model for Alzheimer's β-amyloid fibrils based on experimental constraints from solid-state NMR, *Proc. Natl. Acad. Sci. U. S. A. 99*, 16742−7.
2. Glenner, G. G., and Wong, C. W. (1984) Alzheimer's disease: initial report of the purification and characterization of a novel cerebrovascular amyloid protein, *Biochem. Biophys. Res. Commun. 120*, 885−90.
3. Masters, C. L., Simms, G., Weinman, N. A., Multhaup, G., McDonald, B. L., and Beyreuther, K. (1985) Amyloid plaque core protein in Alzheimer disease and Down syndrome, *Proc. Natl. Acad. Sci. U.S.A. 82*, 4245−9.
4. Eanes, E. D., and Glenner, G. G. (1968) X-ray diffraction studies on amyloid filaments, *J. Histochem. Cytochem. 16*, 673−7.
5. Naiki, H., Higuchi, K., Hosokawa, M., and Takeda, T. (1989) Fluorometric determination of amyloid fibrils in vitro using the fluorescent dye, thioflavin T1, *Anal. Biochem. 177*, 244−9.
6. LeVine, H., 3rd. (1993) Thioflavine T interaction with synthetic Alzheimer's disease β-amyloid peptides: detection of amyloid aggregation in solution, *Protein Sci. 2*, 404−10.
7. Glenner, G. G. (1981) The bases of the staining of amyloid fibers: their physico-chemical nature and the mechanism of their dye-substrate interaction, *Prog. Histochem. Cytochem. 13*, 1−37.
8. Klunk, W. E., Pettegrew, J. W., and Abraham, D. J. (1989) Quantitative evaluation of congo red binding to amyloid-like proteins with a β-pleated sheet conformation, *J. Histochem. Cytochem. 37*, 1273−81.

9. Klunk, W. E., Jacob, R. F., and Mason, R. P. (1999) Quantifying amyloid β-peptide (Aβ) aggregation using the Congo red-Aβ (CR-Aβ) spectrophotometric assay, *Anal. Biochem. 266*, 66−76.
10. Harper, J. D., and Lansbury, P. T., Jr. (1997) Models of amyloid seeding in Alzheimer's disease and scrapie: mechanistic truths and physiological consequences of the time-dependent solubility of amyloid proteins, *Annu. Rev. Biochem. 66*, 385−407.
11. Jarrett, J. T., and Lansbury, P. T., Jr. (1993) Seeding "one-dimensional crystallization" of amyloid: a pathogenic mechanism in Alzheimer's disease and scrapie? *Cell 73*, 1055−8.
12. Soreghan, B., Kosmoski, J., and Glabe, C. (1994) Surfactant properties of Alzheimer's Aβ peptides and the mechanism of amyloid aggregation, *J. Biol. Chem. 269*, 28551−4.
13. Lomakin, A., Chung, D. S., Benedek, G. B., Kirschner, D. A., and Teplow, D. B. (1996) On the nucleation and growth of amyloid β-protein fibrils: detection of nuclei and quantitation of rate constants, *Proc. Natl. Acad. Sci. U.S.A. 93*, 1125−9.
14. Kayed, R., Sokolov, Y., Edmonds, B., McIntire, T. M., Milton, S. C., Hall, J. E., and Glabe, C. G. (2004) Permeabilization of lipid bilayers is a common conformation-dependent activity of soluble amyloid oligomers in protein misfolding diseases, *J. Biol. Chem. 279*, 46363−6.
15. Yong, W., Lomakin, A., Kirkitadze, M. D., Teplow, D. B., Chen, S. H., and Benedek, G. B. (2002) Structure determination of micelle-like intermediates in amyloid β-protein fibril assembly by using small angle neutron scattering, *Proc. Natl. Acad. Sci. U.S.A. 99*, 150−4.
16. Kirkitadze, M. D., Condron, M. M., and Teplow, D. B. (2001) Identification and characterization of key kinetic intermediates in amyloid β-protein fibrillogenesis, *J. Mol. Biol. 312*, 1103−19.
17. Benzinger, T. L., Gregory, D. M., Burkoth, T. S., Miller-Auer, H., Lynn, D. G., Botto, R. E., and Meredith, S. C. (2000) Two-dimensional structure of β-amyloid(10−35) fibrils, *Biochemistry 39*, 3491−9.
18. Benzinger, T. L., Gregory, D. M., Burkoth, T. S., Miller-Auer, H., Lynn, D. G., Botto, R. E., and Meredith, S. C. (1998) Propagating structure of Alzheimer's β-amyloid(10−35) is parallel β-sheet with residues in exact register, *Proc. Natl. Acad. Sci. U.S.A. 95*, 13407−12.
19. Balbach, J. J., Petkova, A. T., Oyler, N. A., Antzutkin, O. N., Gordon, D. J., Meredith, S. C., and Tycko, R. (2002) Supramolecular structure in full-length Alzheimer's beta-amyloid fibrils: evidence for a parallel β-sheet organization from solid-state nuclear magnetic resonance, *Biophys. J. 83*, 1205−16.
20. Antzutkin, O. N., Balbach, J. J., Leapman, R. D., Rizzo, N. W., Reed, J., and Tycko, R. (2000) Multiple quantum solid-state NMR indicates a parallel, not antiparallel, organization of β-sheets in Alzheimer's β-amyloid fibrils, *Proc. Natl. Acad. Sci. U.S.A. 97*, 13045−50.
21. Antzutkin, O. N., Balbach, J. J., and Tycko, R. (2003) Site-specific identification of non-β-strand conformations in Alzheimer's β-amyloid fibrils by solid-state NMR, *Biophys. J. 84*, 3326−35.
22. Antzutkin, O. N., Leapman, R. D., Balbach, J. J., and Tycko, R. (2002) Supramolecular structural constraints on Alzheimer's β-amyloid fibrils from electron microscopy and solid-state nuclear magnetic resonance, *Biochemistry 41*, 15436−50.
23. Malinchik, S. B., Inouye, H., Szumowski, K. E., and Kirschner, D. A. (1998) Structural analysis of Alzheimer's β(1-40) amyloid: protofilament assembly of tubular fibrils, *Biophys. J. 74*, 537−45.
24. Lee, J. P., Stimson, E. R., Ghilardi, J. R., Mantyh, P. W., Lu, Y. A., Felix, A. M., Llanos, W., Behbin, A., Cummings, M., Van Criekinge, M., et al. (1995) ^{1}H NMR of Aβ amyloid peptide congeners in water solution. Conformational changes correlate with plaque competence, *Biochemistry 34*, 5191−200.
25. Zhang, S., Iwata, K., Lachenmann, M. J., Peng, J. W., Li, S., Stimson, E. R., Lu, Y., Felix, A. M., Maggio, J. E., and Lee, J. P. (2000) The Alzheimer's peptide Aβ adopts a collapsed coil structure in water, *J. Struct. Biol. 130*, 130−41.
26. Hou, L., Shao, H., Zhang, Y., Li, H., Menon, N. K., Neuhaus, E. B., Brewer, J. M., Byeon, I. J., Ray, D. G., Vitek, M. P., Iwashita, T., Makula, R. A., Przybyla, A. B., and Zagorski, M. G. (2004) Solution NMR studies of the Aβ(1-40) and Aβ (1-42) peptides establish that the Met35 oxidation state affects the mechanism of amyloid formation, *J. Am. Chem. Soc. 126*, 1992−2005.
27. Ma, B., and Nussinov, R. (2002) Stabilities and conformations of Alzheimer's β-amyloid peptide oligomers (Aβ16-22, Aβ16-35, and Aβ10-35): Sequence effects, *Proc. Natl. Acad. Sci. U.S.A. 99*, 14126−31.
28. Kheterpal, I., Williams, A., Murphy, C., Bledsoe, B., and Wetzel, R. (2001) Structural features of the Aβ amyloid fibril elucidated by limited proteolysis, *Biochemistry 40*, 11757−67.
29. Kheterpal, I., Lashuel, H. A., Hartley, D. M., Walz, T., Lansbury, P. T., Jr., and Wetzel, R. (2003) Aβ protofibrils possess a stable core structure resistant to hydrogen exchange, *Biochemistry 42*, 14092−8.
30. Williams, A. D., Portelius, E., Kheterpal, I., Guo, J. T., Cook, K. D., Xu, Y., and Wetzel, R. (2004) Mapping Aβ amyloid fibril secondary structure using scanning proline mutagenesis, *J. Mol. Biol. 335*, 833−42.
31. Torok, M., Milton, S., Kayed, R., Wu, P., McIntire, T., Glabe, C. G., and Langen, R. (2002) Structural and dynamic features of Alzheimer's Aβ peptide in amyloid fibrils studied by site-directed spin labeling, *J. Biol. Chem. 277*, 40810−5.
32. Luo, P., Braddock, D. T., Subramanian, R. M., Meredith, S. C., and Lynn, D. G. (1994) Structural and thermodynamic characterization of a bioactive peptide model of apolipoprotein E: side-chain lactam bridges to constrain the conformation, *Biochemistry 33*, 12367−77.
33. Felix, A. M., Wang, C. T., Heimer, E. P., and Fournier, A. (1988) Applications of Bop Reagent in Solid-Phase Synthesis. 2. Solid-Phase Side-Chain to Side-Chain Cyclizations Using Bop Reagent, *Int. J. Pept. Protein Res. 31*, 231−8.
34. Gullion, T., and Schaefer, J. (1989) Rotational-Echo Double-Resonance NMR, *J. Magn. Reson. 81*, 196−200.
35. Jaroniec, C. P., Tounge, B. A., Herzfeld, J., and Griffin, R. G. (2001) Frequency selective heteronuclear dipolar recoupling in rotating solids: accurate ^{13}C−^{15}N distance measurements in uniformly ^{13}C,^{15}N-labeled peptides, *J. Am. Chem. Soc. 123*, 3507−19.
36. Ishii, Y., Balbach, J. J., and Tycko, R. (2001) Measurement of dipole-coupled lineshapes in a many-spin system by constant-time two-dimensional solid state NMR with high-speed magic-angle spinning, *Chem. Phys. 266*, 231−6.
37. Haque, T. S., and Gellman, S. H. (1997) Insights on beta-hairpin stability in aqueous solution from peptides with enforced type I′ and type II′ beta-turns, *J. Am. Chem. Soc. 119*, 2303−4.
38. Blanco, F., Ramirez-Alvarado, M., and Serrano, L. (1998) Formation and stability of beta-hairpin structures in polypeptides, *Curr. Opin. Struct. Biol. 8*, 107−11.
39. Espinosa, J. F., Munoz, V., and Gellman, S. H. (2001) Interplay between hydrophobic cluster and loop propensity in beta-hairpin formation, *J. Mol. Biol. 306*, 397−402.
40. Hilbich, C., Kisters-Woike, B., Reed, J., Masters, C. L., and Beyreuther, K. (1991) Aggregation and secondary structure of synthetic amyloid beta A4 peptides of Alzheimer's disease, *J. Mol. Biol. 218*, 149−63.
41. Saito, H. (1986) Conformation-Dependent C-13 Chemical-Shifts—a New Means of Conformational Characterization as Obtained by High-Resolution Solid-State C-13 Nmr, *Magn. Reson. Chem. 24*, 835−52.
42. Wishart, D. S., Bigam, C. G., Holm, A., Hodges, R. S., and Sykes, B. D. (1995) 1H, 13C and 15N random coil NMR chemical shifts of the common amino acids. I. Investigations of nearest-neighbor effects, *J. Biomol. NMR 5*, 67−81.
43. Petkova, A. T., Leapman, R. D., Guo, Z., Yau, W. M., Mattson, M. P., and Tycko, R. (2005) Self-propagating, molecular-level polymorphism in Alzheimer's beta-amyloid fibrils, *Science 307*, 262−5.
44. Weliky, D. P., Bennett, A. E., Zvi, A., Anglister, J., Steinbach, P. J., and Tycko, R. (1999) Solid-state NMR evidence for an antibody-dependent conformation of the V3 loop of HIV-1 gp120, *Nat. Struct. Biol. 6*, 141−5.
45. Petkova, A. T., Buntkowsky, G., Dyda, F., Leapman, R. D., Yau, W. M., and Tycko, R. (2004) Solid state NMR reveals a pH-dependent antiparallel beta-sheet registry in fibrils formed by a beta-amyloid peptide, *J. Mol. Biol. 335*, 247−60.
46. Lansbury, P. T., Jr., Costa, P. R., Griffiths, J. M., Simon, E. J., Auger, M., Halverson, K. J., Kocisko, D. A., Hendsch, Z. S., Ashburn, T. T., Spencer, R. G., et al. (1995) Structural model for the beta-amyloid fibril based on interstrand alignment of an antiparallel-sheet comprising a C-terminal peptide, *Nat. Struct. Biol. 2*, 990−8.
47. Gordon, D. J., Balbach, J. J., Tycko, R., and Meredith, S. C. (2004) Increasing the amphiphilicity of an amyloidogenic peptide changes the beta-sheet structure in the fibrils from antiparallel to parallel, *Biophys. J. 86*, 428−34.

48. Balbach, J. J., Ishii, Y., Antzutkin, O. N., Leapman, R. D., Rizzo, N. W., Dyda, F., Reed, J., and Tycko, R. (2000) Amyloid fibril formation by A beta 16−22, a seven-residue fragment of the Alzheimer's beta-amyloid peptide, and structural characterization by solid-state NMR, *Biochemistry 39*, 13748−59.
49. Pasternack, R. F., Fleming, C., Herring, S., Collings, P. J., dePaula, J., DeCastro, G., and Gibbs, E. J. (2000) Aggregation kinetics of extended porphyrin and cyanine dye assemblies, *Biophys. J. 79*, 550−60.
50. Leyvraz, F. (1986) Rate equation approach to aggregation phenomena, in *On Growth and Form* (Stanley, H. E., and Ostrowski, N., Eds.) pp 136−144, Martinus Nijhoff Publishers, Dordrecht, The Netherlands.
51. Krebs, M. R., Morozova-Roche, L. A., Daniel, K., Robinson, C. V., and Dobson, C. M. (2004) Observation of sequence specificity in the seeding of protein amyloid fibrils, *Protein Sci. 13*, 1933−8.
52. O'Nuallain, B., Williams, A. D., Westermark, P., and Wetzel, R. (2004) Seeding specificity in amyloid growth induced by heterologous fibrils, *J. Biol. Chem. 279*, 17490−9.
53. Esler, W. P., Felix, A. M., Stimson, E. R., Lachenmann, M. J., Ghilardi, J. R., Lu, Y. A., Vinters, H. V., Mantyh, P. W., Lee, J. P., and Maggio, J. E. (2000) Activation barriers to structural transition determine deposition rates of Alzheimer's disease a beta amyloid, *J. Struct. Biol. 130*, 174−83.
54. Kapurniotu, A., Buck, A., Weber, M., Schmauder, A., Hirsch, T., Bernhagen, J., and Tatarek-Nossol, M. (2003) Conformational restriction via cyclization in beta-amyloid peptide Aβ(1-28) leads to an inhibitor of Aβ(1-28) amyloidogenesis and cytotoxicity, *Chem. Biol. 10*, 149−59.
55. Gargani, R. A., Silva, D., Barber-Armstrong, W., and Decatur, S. M. (2003) The Organization and assembly of a β-sheet formed by a prion peptide in solution: An isotope-edited FTIR study, *J. Am. Chem. Soc. 125*, 13674−5.
56. Santini, S., Mousseau, N., Derreumaux, P. (2004) In silico assembly of Alzheimer's Aβ_{16-22} peptide into β-sheets. *J. Am. Chem. Soc. 126*, 11509−16.
57. Tycko, R. (2004) Progress towards a molecular-level structural understanding of amyloid fibrils, *Curr. Opin. Struct. Biol. 14*, 96−103.
58. Hasegawa, K., Yamaguchi, I., Omata, S., Gejyo, F., and Naiki, H. (1999) Interaction between A beta(1-42) and A beta(1-40) in Alzheimer's beta-amyloid fibril formation in vitro, *Biochemistry 38*, 15514−21.
59. Iwata, K., Eyles, S. J., and Lee, J. P. (2001) Exposing asymmetry between monomers in Alzheimer's amyloid fibrils via reductive alkylation of lysine residues, *J. Am. Chem. Soc. 123*, 6728−9.
60. Gordon, D. J., Sciarretta, K. L., and Meredith, S. C. (2001) Inhibition of beta-amyloid(40) fibrillogenesis and disassembly of beta-amyloid(40) fibrils by short beta-amyloid congeners containing N-methyl amino acids at alternate residues, *Biochemistry 40*, 8237−45.

BI0474867